Oikos

O16034

Bigler, C., Gavin, D. G. ,Gunning, C. and Veblen, T. T. 2007. Drought induces lagged tree mortality in a subalpine forest in the Rocky Mountains. – Oikos 116: 1983–1994.

Appendix A1. Estimation of monthly mean temperature and precipitation for the Cameron Pass study area, Colorado.

Long-term climate data from seven climate stations were available from the Western Regional Climate Center (WRCC, http://www.wrcc.dri.edu/summary/climsmco.html) and from two high-elevation climate stations from the Niwot Ridge Long-Term Ecological Research Site (INSTAAR, Boulder, USA, http://culter.colorado.edu/NWT) (Table A1.1). We considered only months with no missing precipitation days and with < 5 missing temperature days (WRCC data) or ≥ 24 available temperature days (INSTAAR data). Monthly lapse rates were computed from linear regressions of mean temperature and precipitation (over the period of record) versus elevation. In addition to the nine climate stations (Table A1.1), four climate stations below 2310 m (Estes Park, Hayden, Kremmling, Steamboat Springs) were used to calculate temperature lapse rates, and two of these stations (Estes Park, Kremmling) were used to calculate precipitation lapse rates (Table A1.2). Exploratory analyses suggested there was no long-term trend in lapse rates, thus supporting the use of a single monthly lapse rate over the entire period of record at each site. Temperature lapse rates were shallow in winter (ca –2.6°C km^{-1}), probably due to frequent temperature inversions, but steep in summer (ca –5.6°C km^{-1}) with little variation from predicted values ($R^2 > 0.83$; Table A1.2). Precipitation lapse rates were steeper in winter (ca 50.1 mm km^{-1}) than in summer (ca 16.1 mm km^{-1}).

For the nine climate stations (Table A1.1), we adjusted temperature and precipitation to the elevation of the study area close to Cameron Pass (3141 m a.s.l.) using the monthly lapse rates. The lapse-rate corrected temperature and precipitation values were averaged by weighting each station by the inverse distance to Cameron Pass (Cook et al. 1999).

Although the only climate stations that covered the period from 1910 to 1948 (Dillon and Fraser) were relatively far away from the study area (Table A1.1), these two climate stations are likely representative for the study area. Median correlations for the lapse-rate corrected monthly climate data between the climate stations Dillon and Fraser and the two climate stations that were closest to the study area (Grand Lake 1 and Hourglass Reservoir) ranged between 0.80 to 0.87 for temperature and between 0.50 to 0.77 for precipitation.

Reference

Cook, E. R. et al. 1999. Drought reconstructions for the continental United States. – J. Clim. 12: 1145–1162.

Table A1.1. Climate stations in the region near Cameron Pass, Colorado.

Station name	Latitude (N)	Longitude (W)	Elevation (m)	Distance to Cameron Pass (km)	Period of record (year)
Allenspark Lodge	40°12′00′′	105°32′00′′	2560	46.4	1948 – 1993
Dillon 1E	39°38′00′′	106°02′00′′	2741	103.3	1910 – 2004
Fraser	39°57′00′′	105°50′00′′	2609	66.7	1910 – 1974
Grand Lake 1 NW	40°16′00′′	105°50′00′′	2620	19.6	1948 – 2004
Grand Lake 6 SSW	40°11′00′′	105°52′00′′	2540	40.8	1948 – 2004
Hourglass Reservoir	40°38′00′′	105°36′00′′	2902	21.8	1988 – 2004
Niwot Ridge C-1	40°02′09′′	105°32′09′′	3018	62.5	1952 – 2004
Niwot Ridge D-1	40°03′34′′	105°37′00′′	3743	57.5	1952 – 2004
Red Feather Lakes 2 SE	40°47′00′′	105°33′00′′	2520	35.2	1948 – 1990

Table A1.2. Lapse rates computed from monthly mean climate data using linear regression.

Month	Temperature (°C km^{-1})				Precipitation (mm km^{-1})			
	Coeff.	SE	p	R^2 (adj.)	Coeff.	SE	p	R^2 (adj.)
January	–2.1	1.9	0.298	0.02	55.1	8.6	< 0.001	0.80
February	–3.3	1.6	0.072	0.20	52.6	6.2	< 0.001	0.88
March	–5.0	1.1	0.001	0.61	64.0	5.4	< 0.001	0.93
April	–6.5	0.6	< 0.001	0.91	64.2	8.1	< 0.001	0.86
May	–6.2	0.5	< 0.001	0.94	33.6	10.8	0.013	0.46
June	–5.6	0.6	< 0.001	0.87	17.6	7.2	0.037	0.33
July	–5.5	0.7	< 0.001	0.83	16.0	9.8	0.138	0.14
August	–5.6	0.7	< 0.001	0.84	14.6	5.5	0.026	0.38
September	–5.2	0.7	< 0.001	0.83	17.0	3.9	0.002	0.65
October	–5.0	0.8	< 0.001	0.75	23.2	4.1	< 0.001	0.75
November	–4.5	1.1	0.002	0.55	53.1	5.0	< 0.001	0.92
December	–2.5	1.8	0.184	0.08	42.5	7.7	< 0.001	0.75

Note: shown are regression coefficients, standard errors (SE), p-values, and adjusted R^2 (n temperature = 13, n precipitation = 11).

Appendix A2. Calculation of monthly water deficits for the study area.

We computed the soil water balance for the study area using a modified Thornthwaite method described in Willmott et al. (1985). The soil water balance is modelled on a daily time step by estimating soil-water withdrawal, recharge, and surplus. Soil-water withdrawal (or actual evapotranspiration, AE) is estimated from potential evapotranspiration (PE) and the percentage the current soil is at the available water capacity (AWC). Monthly potential evapotranspiration is estimated empirically from monthly mean temperature and day length. Daily PE is based on monthly PE distributed evenly over the month. AE is computed by multiplying PE by a 'declining availability function', which assumes once soil water drops below < 30% of AWC, the proportion of PE that is actually transpired quickly drops to zero. This function assumes that as soil water is drawn down during the summer, it is increasingly difficult to extract due to cohesion by soil particles. AWC at Cameron Pass is approximately 75 mm based on soil survey data (US Forest Service). Soil-water recharge occurs on days when snowmelt and/or precipitation exceed soil-water withdrawal. When soil-water is at AWC, any snowmelt and precipitation beyond that required by PE is considered surplus and is not available on following days. Daily snowmelt is empirically estimated from the temperature, the amount of accumulated snow and daily precipitation, which is based on monthly precipitation distributed evenly over the month. We computed the water balance using a custom program following Willmott et al. (1985) (freely available at http://geography.uoregon.edu/gavin/software.html). The lapse-rate corrected temperature and precipitation values (Appendix A1) were used to calculate monthly and cumulative monthly water deficits for the study area (Fig. A2.1). Early-season water deficits were defined as cumulative monthly water deficits from January through July, late-season water deficits were defined as cumulative monthly water deficits from January through December (Fig. A2.1b).

Water deficits generally start building up during the growing period from June to October (Fig. A2.1b). An observed late-season water deficit of 100 mm corresponds to approximately 14% of the average annual precipitation (697 mm), and a water deficit of 60 mm corresponds to about 9% of the annual sum. Similarly, a water deficit of 40 mm through July approximates 9% of the average precipitation through July (444 mm), and a water deficit of 20 mm corresponds to about 5% of the sum through July.

Reference

Willmott, C. J., Rowe, C. M. and Mintz, Y. 1985. Climatology of the terrestrial seasonal water cycle. – J. Climatol. 5: 589–606.

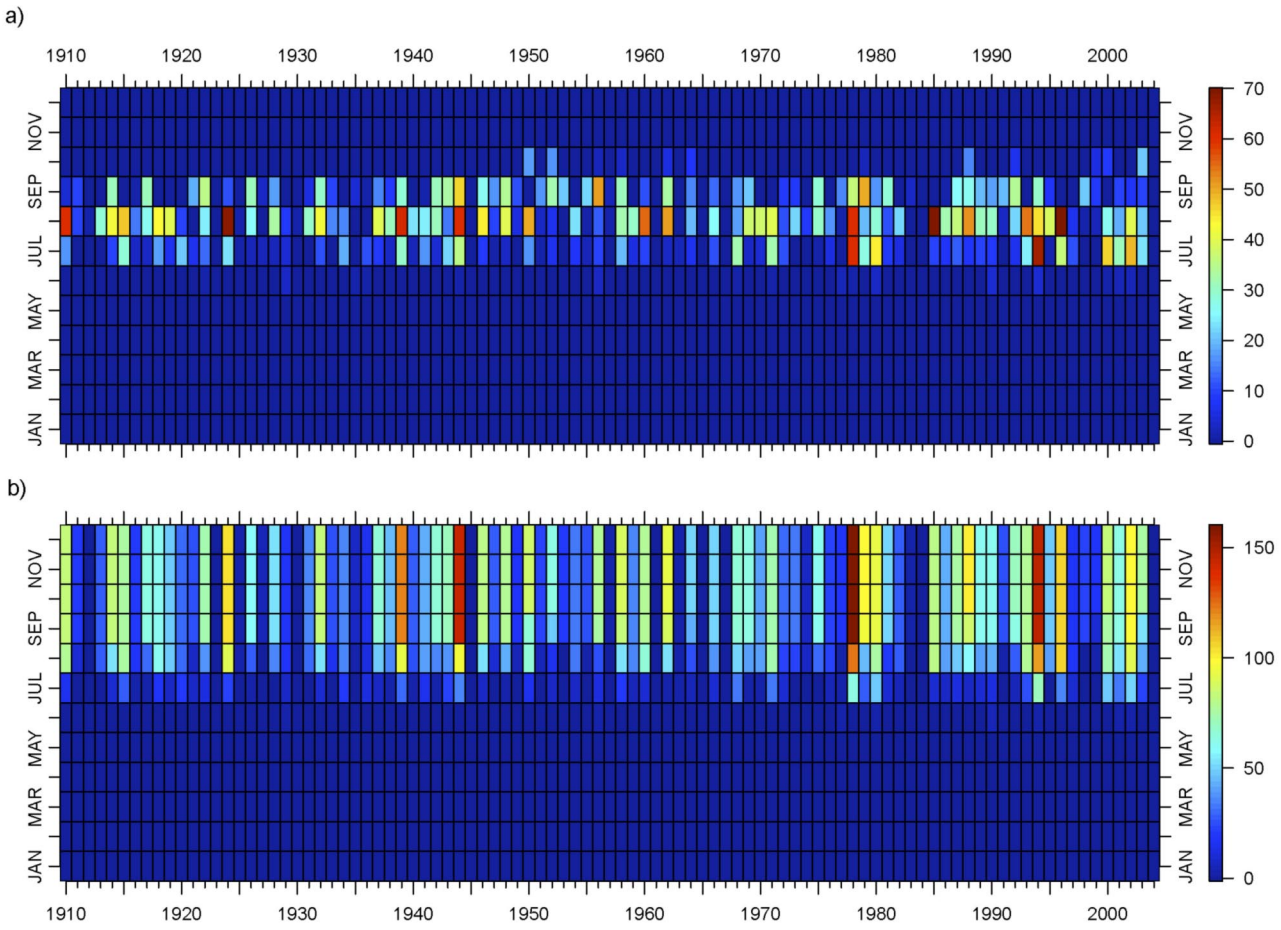

Fig. A2.1. Monthly and cumulative monthly water deficits.
Water deficits (mm) are shown for the period 1910 to 2004 as: a) monthly values, and b) cumulative monthly values.

Appendix A3. Bivariate event date analysis for simulated, causally-related series of events.

Visual comparison of two series of events such as tree mortality and drought might suggest a direct relationship between these two records (Fig. 1). However, to detect more complex relationships between two causally-related series, statistical methods need to be taken into account. Superposed epoch analysis (Chree 1913, Baisan and Swetnam 1990), which is commonly used to compare values of a series (e.g. drought index) during event and non-event years (e.g. mortality or fire events), can be used to examine variations in the independent variable (e.g. drought) for different time lags before or after the event dates. However, this method is not able to summarise the overall, cumulative effect of series A on series B within a particular lag, such as lagged mortality over several years after drought. Furthermore, in the case of correlation analysis that is sometimes used to compare trends in two series, temporal autocorrelation often occurs in one or both of the series which can bias variances and lead to incorrect statistical inference. Using event date analysis, complex patterns such as long-lasting lag effects or overlapping lags can be detected at different temporal scales.

The following simple example shows, how values for $K_{DM}(t)$ and $L_{DM}(t)$ are calculated for different lags t. We assume that two droughts (D) occurred between 1910 and 1920: drought D1 in 1910 and drought D2 in 1916 (Fig. A3.1). We further assume that five mortality events (M) occurred during this period, M1 and M2 in 1910, M3 in 1911, M4 in 1916, and M5 in 1917 (Fig. A3.1). To calculate values for $L_{DM}(t)$, the following parameters are needed (Eq. 1 in the text): length T of the record = 11, number of drought events $n_D = 2$, number of mortality events $n_M = 5$, and $T/(n_D\, n_M) = 1.1$. In this example, the values for $L_{DM}(t)$ increase from lag 0 to lag 1 and then decrease to lag 5 (Table A3.1).

To illustrate the power of event date analysis, we generated eight data sets of two causally-related series of events A and B, whereas event B followed event A within a predetermined lag. The same period (1910 – 2004) and similar number of A and B events was used to make these simulations comparable to the drought-mortality data, where drought would be represented by event A and mortality by event B. After 5 or 20 A event years were randomly selected from a uniform distribution (i.e., the time series were stationary and did not include any trend), 20 or 50 B events were randomly selected that followed the A events within a lag of up to 5 or 15 years. B events that occurred after 2004 were omitted, and therefore, the number of B events differed from 20 or 50 in some simulations. Event date analysis (Eq. 1 in the text) was performed, and the calculated $L_{AB}(t)$ values were compared with 95% and 99% confidence envelopes that were derived from 1000 Monte-Carlo simulations (Fig. A3.2).

Most of the significant lags were close to the selected lag. However, some results showed some variability, e.g. in one case, the significant lags varied from 4 to 13 years around the true lag of 5 years (Fig. A3.2a). However, these examples show only the outcome of one simulated data set each, and the resulting actual lags depend on the specific data sets of A and B events, where the relative positions of the A events to each other also affect the results.

References

Chree, C. 1913. Some phenomena of sunspots and of terrestrial magnetism at Kew Observatory. – Philos. Trans. R. Soc. Lond. A 212: 75–116.

Baisan, C. H. and Swetnam, T. W. 1990. Fire history on a desert mountain range: Rincon Mountain Wilderness, USA. – Can. J. For. Res. 20: 1559–1569.

Table A3.1. Calculation of $K_{DM}(t)$ and $L_{DM}(t)$ for lags 0 to 5.

t	$n_{D1}(t)$	$n_{D2}(t)$	$n_D(t)$	Mortality events	$K_{DM}(t)$	$L_{DM}(t)$
0	2	1	3	M1, M2, M4	3.3	3.3
1	3	2	5	M1, M2, M3, M4, M5	5.5	4.5
2	3	2	5	M1, M2, M3, M4, M5	5.5	3.5
3	3	2	5	M1, M2, M3, M4, M5	5.5	2.5
4	3	2	5	M1, M2, M3, M4, M5	5.5	1.5
5	3	2	5	M1, M2, M3, M4, M5	5.5	0.5

Note: the term $n_{D1}(t)$ shows the number of mortality events during and following drought D1, $n_{D2}(t)$ shows the number of mortality events during and following drought D2, and $n_D(t)$ shows the number of mortality events during and following drought D1 and D2.

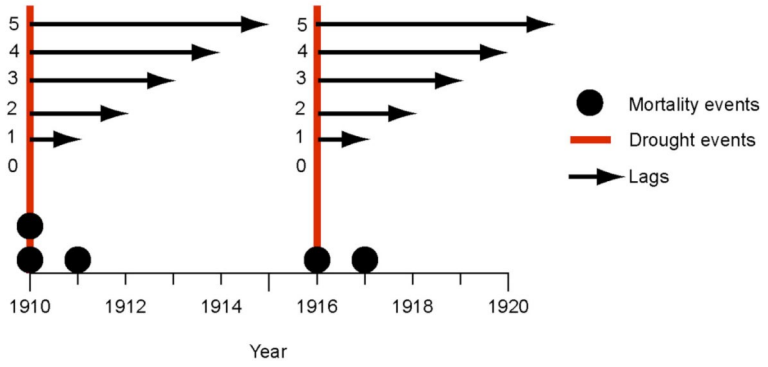

Fig. A3.1. Example of bivariate event date analysis.
Shown are two drought events in 1910 and 1916 (vertical, red lines) followed by five mortality events (black dots). The arrows indicate lags 0 to 5.

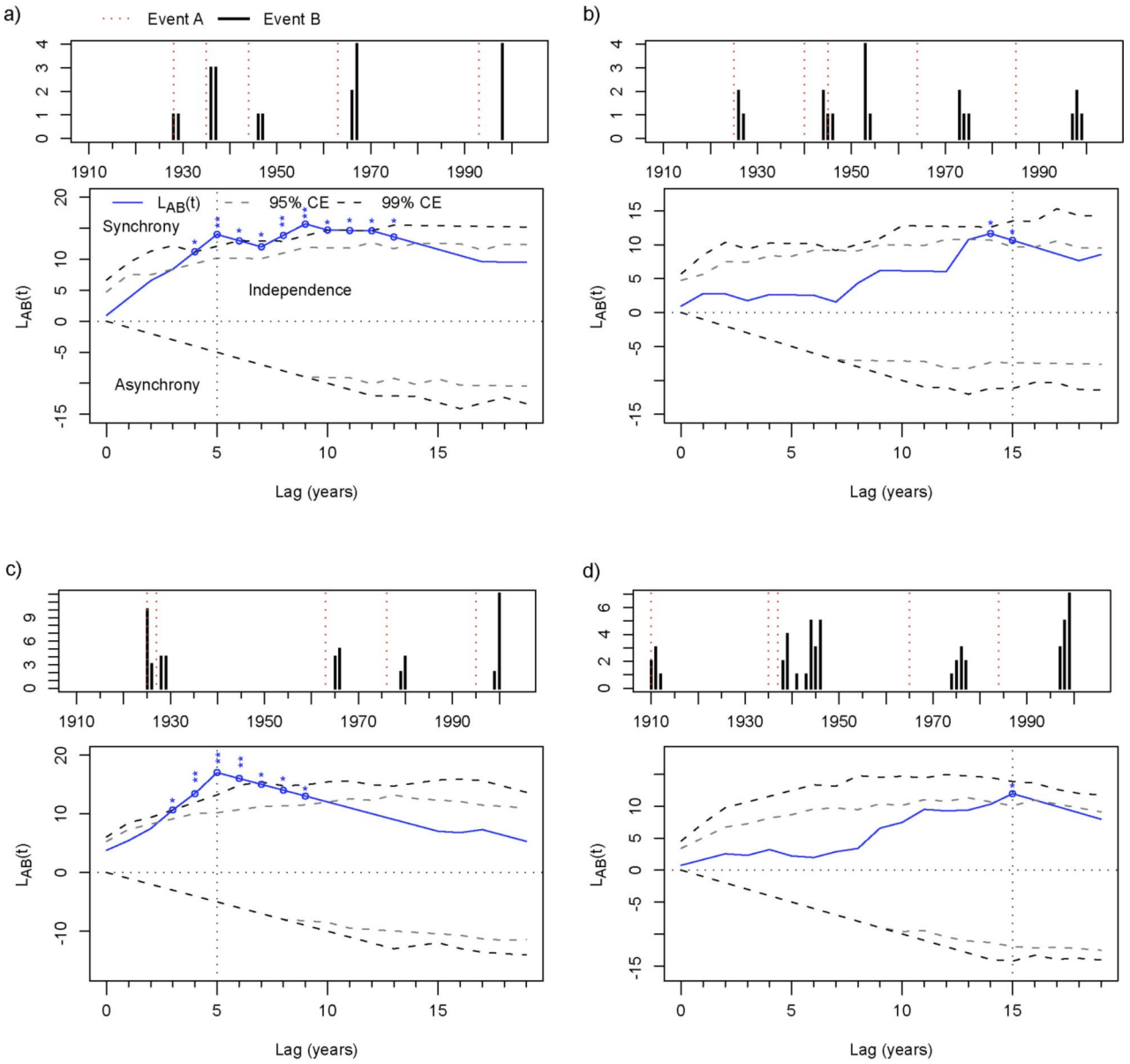

Fig. A3.2. Bivariate event date analysis with simulated data. The histograms (upper panels) show the simulated A events (red, dotted lines) and number of B events (black bars). In these simulations, B follows A with lags up to 5 or 15 years over the period 1910 to 2004. The line plots (lower panels) show the resulting values of $L_{AB}(t)$ (blue, solid line) and 95% confidence envelopes (CE; grey, dashed lines) and 99% confidence envelopes (CE; black, dashed lines). The dotted, vertical lines denote the selected lags. Values of $L_{AB}(t)$ above the upper confidence limits show synchrony, values below the lower confidence limits show asynchrony, and values between the confidence limits show independence between the two series of events. Significant lags are marked (*, $p < 0.05$; **, $p < 0.01$). Results are shown for the following simulated data sets: (a) 5 A events, 20 B events, lag = 5 years; (b) 5 A events, 20 B events, lag = 15 years; (c) 5 A events, 50 B events, lag = 5 years; (d) 5 A events, 50 B events, lag = 15 years; (e) 20 A events, 17 B events, lag = 5 years; (f) 20 A events, 17 B events, lag = 15 years; (g) 20 A events, 38 B events, lag = 5 years; (h) 20 A events, 41 B events, lag = 15 years.

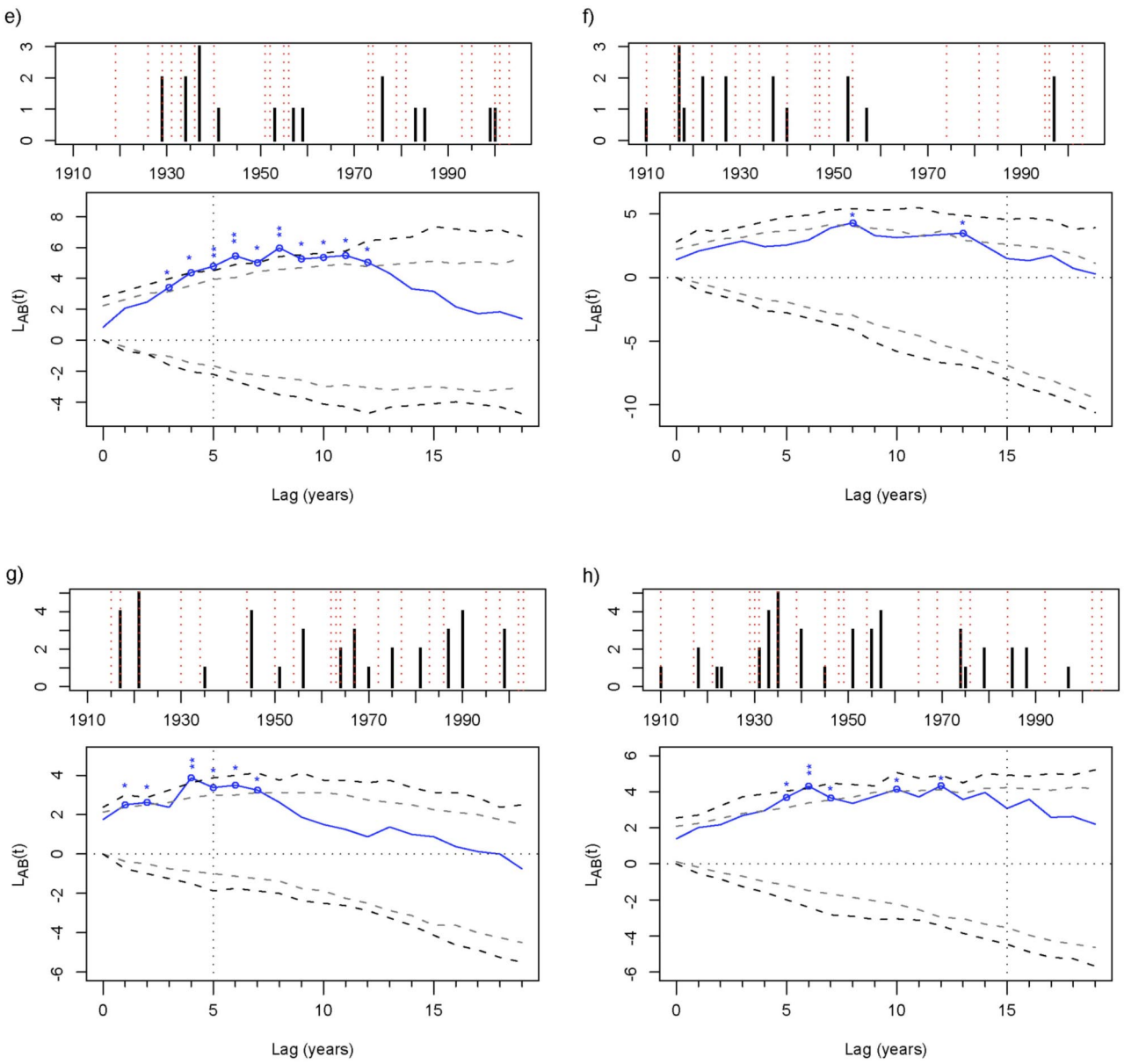

Fig. A3.2. Continued.